

# Folded Sub-1 V $V_\pi$ Thin Film Lithium Niobate Phase Modulator

Xiaofeng Zhu<sup>1</sup>, Marco Moller de Freitas<sup>1</sup>, Shouyuan Shi<sup>1</sup>, *Member, IEEE*, Peng Yao, Fuquan Wang, Christopher J. Cullen, Maxwell Hinkle<sup>2</sup>, and Dennis W. Prather<sup>1</sup>, *Fellow, IEEE*

**Abstract**—This work reports a sub-1 volt drive voltage ( $V_\pi$ ) folded phase modulator utilizing capacitor-loaded traveling wave electrodes (CLTWEs). The implementation employs a low-loss CLTWE on a quartz (Qz) substrate, facilitating both broadband index matching and minimal RF loss. A series of phase modulators of varying lengths have been fabricated and subjected to experimental characterization. The measured loss for straight CLTWEs is 0.21 dB/(cm·GHz<sup>1/2</sup>). The experimentally determined DC  $V_\pi$  is 0.52 V for a modulation length of 7.5 cm.

**Index Terms**—TFLN, phase modulator, CLTWE, low  $V_\pi$ .

## I. INTRODUCTION

MICROWAVE photonic links (MPLs) and radio-frequency-over-fiber (RFoF) systems leverage low loss optical domain transport of RF signals over large distances, particularly in the millimeter wave (mmW) frequency range. This enables extremely high data rates and immunity to electromagnetic interference. In this context, electro-optical modulators (EOMs) represent a key device for these advanced systems. However, to deliver practical devices for this application, essential performance requirements such as low driving voltage, high efficiency, and compact footprint are necessary.

Numerous studies have been presented in the literature to realize a small footprint, low drive voltage, and high-bandwidth EOM on various material platforms such as silicon [1] and indium phosphide [2]. Compared with these material systems, Lithium niobate (LN) is a more promising material for electro-optic modulation due to its relatively strong Pockels effect ( $r_{33} = 30.8$  pm/V) and a broad transparency window ranging from the visible to the mid-infrared spectrum [3], [4]. LN has also shown better performance in terms of  $V_\pi$ , bandwidth, optical loss, nonlinear response, power handling, and long-term

stability [5]. Recently, a large bandwidth (>500 GHz) [6] and low  $V_\pi$  (<1 V) have been experimentally demonstrated in an LN-on-insulator (LNOI) EOM. There have been reported modulators exhibiting a small footprint and having low  $V_\pi \cdot L_S$ , through cavity-enhanced [7] and plasmonic modulators [8], however, these devices still exhibit a high  $V_\pi$  value due to their relatively short modulation region. State of the art modulators have shown a  $V_\pi$  value of 1 V,  $V_\pi \cdot L$  of 2 V·cm, and a 3-dB bandwidth around 100 GHz with a long device length of 2 cm [9]. The long interaction length enables near sub-1 volt  $V_\pi$ , however, this adds additional challenges, such as increased device footprint, as well as increased difficulty in matching the RF and optical mode index. However, these sub-1 volt  $V_\pi$  devices allow for the reallocation of high-gain MPLs, wideband frequency combs [10], and high-sensitivity photonic-based imagers [11].

In this work, an optimized device is presented based on state of the art  $V_\pi \cdot L$  of 2 V·cm using CLTWE in Qz [9]. Accordingly, the device has been designed with a low-loss transition and a folding structure to minimize the overall footprint of the device. The total length of the device is 7.5 cm, where multiplefolding regions have been fabricated and characterized. Existing TFLN modulators from the literature have reported  $V_\pi$  values of 4, 1.24, 0.7, 2.6, and 1.08 V [12], [13], [14], [15], [16] for MZM platforms, and 1.52 V [10] for a phase modulator. In comparison, the device presented here demonstrates an ultra-low  $V_\pi$  of 0.52 V as a phase-only modulator with a single modulation arm, which has been fabricated to simplify the fabrication and characterization process. In future work, a waveguide crossing [12] will be used to further reduce  $V_\pi$  to approximately 0.25 V by extending the modulation region.

## II. DEVICE DESIGN AND SIMULATION

A single mode ridge-etched thin-film lithium niobate (TFLN) modulator was simulated using Ansys Lumerical Mode solver, which has a 1  $\mu\text{m}$  wide and 300 nm thick ridge on a 300 nm slab. The design achieved over 80% mode confinement and reduced loss caused by the sidewall roughness by tightly confining the optical mode more into the slab. The optical waveguide has a group index of 2.23. In this device, the optical group index can be tuned by changing the thickness of the cladding layer. Considering both fabrication tolerances, modulation efficiency and to minimize the interaction between the optical guided mode

Received 30 September 2024; revised 11 February 2025; accepted 17 February 2025. Date of publication 20 February 2025; date of current version 26 February 2025. This work was supported in part by the Air Force Office of Scientific Research (AFOSR) and the Office of Naval Research (ONR) and in part by the staff at Phase Sensitive Innovation (PSI) and the University of Delaware Nanofabrication Facility (UDNF). (Corresponding author: Xiaofeng Zhu.)

Xiaofeng Zhu, Marco Moller de Freitas, Shouyuan Shi, and Dennis W. Prather are with the Electrical and Computer Engineering Department, University of Delaware, Newark, DE 19716 USA (e-mail: xzhu@udel.edu).

Peng Yao, Fuquan Wang, Christopher J. Cullen, and Maxwell Hinkle are with Phase Sensitive Innovations Inc., Newark, DE 19713 USA.

Color versions of one or more figures in this letter are available at <https://doi.org/10.1109/LPT.2025.3544127>.

Digital Object Identifier 10.1109/LPT.2025.3544127

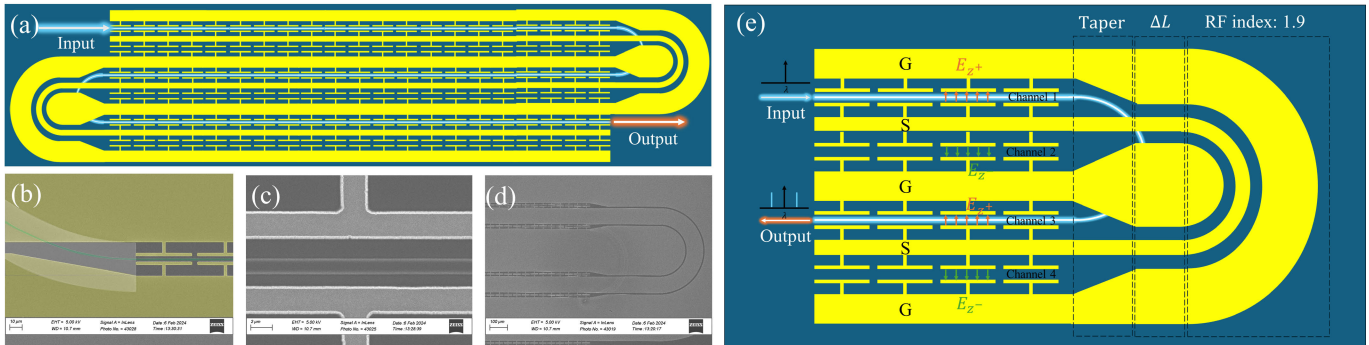


Fig. 1. (a) Figure 4: The layout of the folded phase modulator with single arm modulation, where the optical signal is coupled into the device through the first gap of the electrode (labeled in blue) and folded twice then coupled out (labeled in red). (b) The top-down view of the transition from CLTWE to conventional CPW, in which different material layers have been colored. (c) The TFLN optical waveguide aligns with the T-rail of the CLTWE. (d) the overview of the 180° bending on the thicker oxide cladded optical waveguide. (e) the layout of the bending region.

and the patterned electrodes, a layer of SiO<sub>2</sub> is added to the TFLN layer as a buffer. Based on this concept, the optical waveguide was designed and optimized. For the RF electrodes, a CLTWE structure was used due to its low loss and tunable RF phase index. In our previous work [9], the stem length of the T-rail has shown significant impact on the phase index, which can tune the RF phase index over a range of 2.0 to 2.3. Figure. 1 (a) shows the overview layout of the folded phase modulator using CLTWEs for the modulation region and tapered regions into the conventional coplanar waveguide (CPW). Since the bending electrodes are patterned on top of the optical waveguide, a 500 nm thick SiO<sub>2</sub> was used near the bending region to avoid metal absorption loss, shown in Fig. 1(b-d). The transition from CLTWEs to conventional CPWs in the folded sections helps reduce RF loss in the RF folds. It also maintains a similar signal electrode width and ensures the characteristic impedance of 50 ohms is matched between the CL-TWEs and CPWs. After the transition, the gap between the signal and ground electrodes in the CPW is increased to 10 μm to further reduce RF loss. As shown in Fig. 1 (e), after folding, the optical waveguide must switch from channel 1 to channel 3 due to the reversed crystal directions, which consequently introduces a path difference between the optical and RF paths. The RF index of the conventional CPW is simulated to be 1.9. Since the CPW has a lower RF index, an additional path length of is incorporated to match the total electrical path between the RF and optical signals. As shown in Fig. 2 (a), the transition region of CLTWE was simulated using ANSYS high frequency structure simulator (HFSS), demonstrating a smooth transition of the RF mode. A 2 cm long CLTWE was then fabricated and characterized in the cases with and without transition taper using the Keysight Vector Network Analyzer (VNA). As shown in Fig.2 (b), the taper exhibited negligible losses across the 1 to 50 GHz range, with -20 dB return loss confirming adequate impedance matching.

### III. FABRICATION

A 600 nm thick X-cut TFLN with 2 μm buried oxide (box) on a Qz handle substrate supplied by NanoLN was used to fabricate this device. A 150 nm thick TiW layer was sputtered

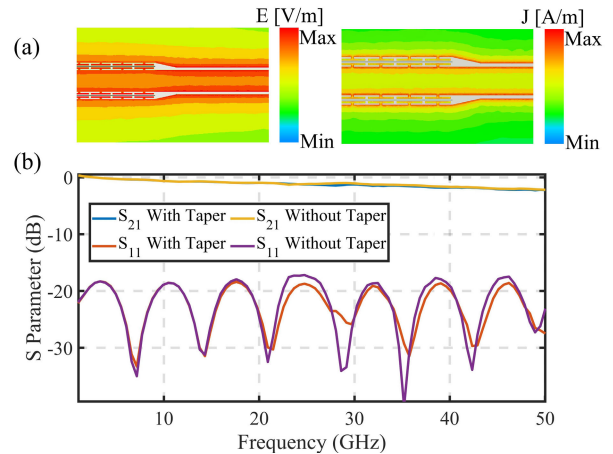


Fig. 2. (a) Left and Right simulations show the electrical field and surface current of transition from CLTWE to conventional CPW in log scale at 100 GHz, respectively. (b) Experimentally measured S parameters of the fabricated CLTWE with and without taper transition.

using a bilayer liftoff process with LOR3A and ARP6200.04 [17]. After liftoff of the alignment marker, a 100 nm Cr was uniformly deposited across the entire sample. Following that, 80 nm thick EBL photoresist ARN7520.073 was spun, baked, and exposed. The EBL writing process was optimized by applying the proximity effect correction (PEC) and multi-pass functions. After the first layer of pattern transfer, the entire sample is cladded with 500 nm thick PECVD SiO<sub>2</sub>. The sample was then back-etched to 186 nm, except for the bending region. Finally, a 10 nm Ti layer and an 800 nm gold layer were then deposited using a dual beam evaporator. After fabrication, the sample was diced and polished for characterization.

## IV. EXPERIMENTAL RESULTS AND DISCUSSION

### A. CLTWE Characterization

The S-parameters of the CLTWEs with different lengths were first characterized using a Keysight VNA, in which two port S parameters, i.e., S<sub>21</sub>, S<sub>12</sub>, S<sub>11</sub> and S<sub>22</sub>, were collected after the STOL calibration process. Figure 5 shows the measured electrode losses for device lengths of 1, 2.5, 5.0 and 7.5 cm. Two shorter devices, 1 cm and 2.5 cm long modulators, have only straight CLTWEs,

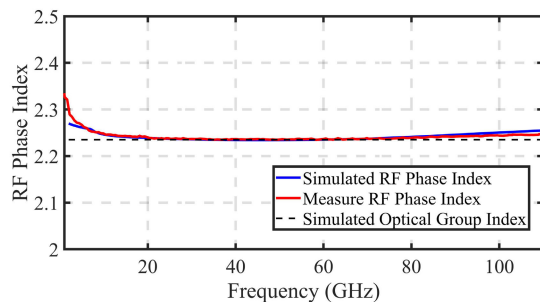


Fig. 3. Comparison among the simulated optical waveguide group index, the simulated RF phase index, and the extracted RF phase index from measured S parameters.

whereas the 5 cm long and 7.5 cm long devices have one and two sets of  $180^\circ$  folded coplanar waveguides (CPWs) and taper transitions, respectively. As discussed previously, the losses caused by the transitions are negligible from 1 to 50 GHz. Using the cut-back method, the bending loss is calculated to be  $3.9 \text{ dB}/(\text{cm}\cdot\text{GHz}^{1/2})$  and straight CLTWE is  $0.21 \text{ dB}/(\text{cm}\cdot\text{GHz}^{1/2})$ . Additionally, the RF phase index of the CLTWE was calculated using the measured S-parameters of the 2.5 cm device. As shown in Fig. 3, the simulated optical group index at 1550 nm is 2.23, which aligns with the simulated RF phase index and the measured RF phase index.

### B. Optical Loss Characterization

The passive section of this device was characterized using a 1550 nm tunable laser through end-butt coupling. The laser was connected to the  $1 \times 4$  V-Groove lensed fiber; the facet optical signal was coupled to the polished device through the edge. Due to the hardness difference between the Qz handle and TFLN, it is still difficult to achieve a smooth facet through the polishing process. The on-chip loss is approximately 28 dB, with over 20 dB of this loss attributed to coupling loss. Since the mode size of the  $1 \mu\text{m}$  TFLN waveguide is much smaller than that of the lensed fiber, an improved coupling structure is required to reduce the coupling loss. To this end, a dual-layer inverse taper is introduced [18]. In addition, the optical waveguide loss was characterized using a Miro-ring resonator (MRR), where the optical waveguide loss of  $0.5 \text{ dB}/\text{cm}$  was calculated from the Q factor [19].

### C. DC $V_\pi$ Characterization

To characterize the phase modulators, the CWL was connected to a ThorLabs 50:50 splitter to the split the optical signal into two arms. One arm includes the device under test (DUT) and the other was connected to a ThorLabs optical attenuator. The attenuator was tuned to match the optical power through the DUT leg to allow for better extinction through the combiner that follows both legs, allowing for better device performance measurements. The attenuated optical power along with device output signal are then combined and fed into a photodetector (PD). After the optical power was converted to an electrical signal, it was amplified by a transimpedance amplifier (TIA) and connected to an oscilloscope. The DC signal was applied using a function

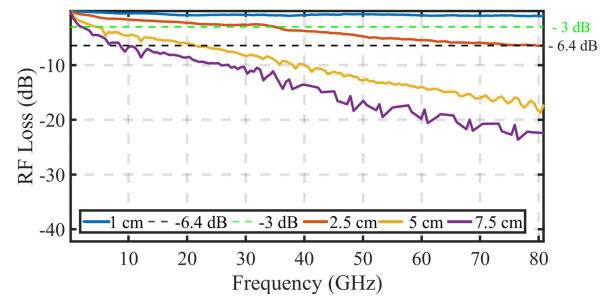


Fig. 4. Experimentally measured RF electrode loss for all different length of electrodes (1, 2.5, 5, and 7.5 cm), wherein the 5 cm long electrode device and the 7.5 cm long device have one and two  $180^\circ$  bends.

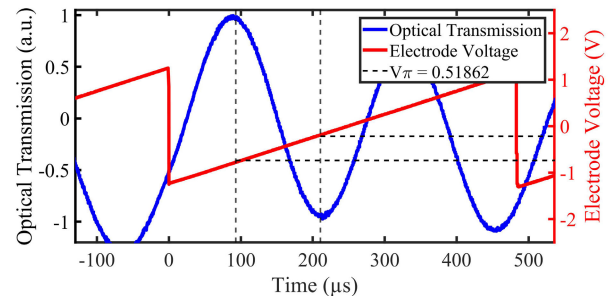


Fig. 5. Experimentally measured DC  $V_\pi$  at 2 KHz, the blue trace is the normalized optical transmission and the red trace is the voltage applied on the device though DC probe.

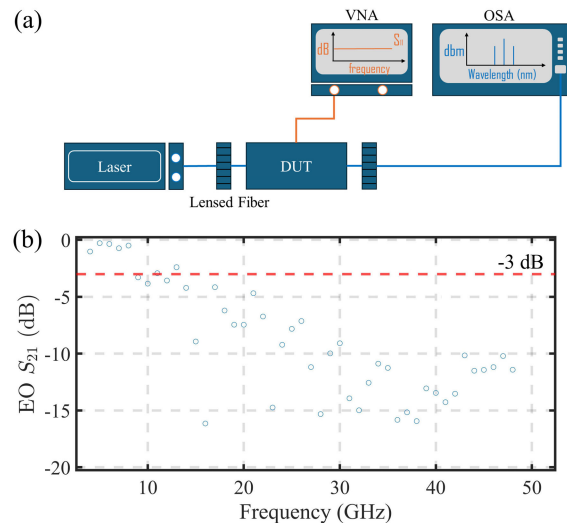


Fig. 6. (a) The block diagram of the optical sideband measurement setup for this electro-optic modulator; (b) The measured electro-optic  $S_{21}$  from 1 to 50 GHz.

generator and triggered with an oscilloscope. As shown in Fig. 5, the blue trace is normalized optical transmission and the red trace is the applied voltage. A  $V_\pi$  of 0.52 V was experimentally measured for the 7.5 cm long device at 2KHz.

### D. High Frequency Characterization

As shown in Fig. 6 (a), the electro-optical response was characterized by using a VNA as an RF source and carrier signal at 1550 nm. Cable loss was first measured by the VNA, which has been normalized through response calibration. The

loss of cable was then imported into the LABVIEW program that control the VNA such that 0 dBm RF power is always launched into the GSG probe. The optical signal from the tunable laser was set to be 1550 nm. The laser was butt coupled into the device with fiber-to-chip alignment. The GSG probe launched the RF signal along the same direction as the optical signal, to have co-propagating modulation. The output signal was collected by an Apex optical spectrum analyzer (OSA), and both the lower and upper sidebands were collected for each frequency. From the modulation equation, in the case of precise index and impedance match, the  $-6.4$ -dB point of electrode RF loss represents the 3-dB point of the EO response [20]. As shown in Fig. 4, the estimated 3-dB bandwidth for the 7.5 cm long device is around 10 GHz. As shown in Fig. 6 (b), the experimentally measured EO  $S_{21}$  with fitting curve has shown the 3-dB bandwidth of 10 GHz for the 7.5 cm long device. The linear roll-off shows that the optical group index and RF phase index are aligned well even after  $180^\circ$  folding for such long devices. Due to the trade off between the  $V_\pi$  and 3-dB bandwidth, the longer device shows reasonable roll-off, which is caused by the RF electrode loss.

## V. CONCLUSION

In this letter, we experimentally demonstrated compact fold sub-1  $V_\pi$  phase modulator using folded CLTWEs with modulation length of 7.5 cm. The  $V_\pi$  of 0.52 and the 3-dB bandwidth of 10 GHz have been experimentally measured.

## REFERENCES

- [1] G. T. Reed, G. Mashanovich, F. Y. Gardes, and D. J. Thomson, "Silicon optical modulators," *Nature Photon.*, vol. 4, no. 8, pp. 518–526, 2010. [Online]. Available: <https://www.nature.com/articles/nphoton.2010.179>
- [2] J. Ozaki et al., "Over-85-GHz-bandwidth InP-based coherent driver modulator capable of 1-Tb/s/ $\lambda$ -Class operation," *J. Lightw. Technol.*, vol. 41, no. 11, pp. 3290–3296, Jun. 1, 2023. [Online]. Available: <https://ieeexplore.ieee.org/document/10017358/?arnumber=10017358>
- [3] C. Li et al., "High modulation efficiency and large bandwidth thin-film lithium niobate modulator for visible light," *Opt. Exp.*, vol. 30, no. 20, p. 36394, Sep. 2022. [Online]. Available: <https://opg.optica.org/oe/abstract.cfm?uri=oe-30-20-36394>
- [4] B. Desiatov, A. Shams-Ansari, M. Zhang, C. Wang, and M. Lončar, "Ultra-low-loss integrated visible photonics using thin-film lithium niobate," *Optica*, vol. 6, no. 3, p. 380, Mar. 2019. [Online]. Available: <https://opg.optica.org/optica/abstract.cfm?uri=optica-6-3-380>
- [5] D. Zhu et al., "Integrated photonics on thin-film lithium niobate," *Adv. Opt. Photon.*, vol. 13, no. 2, pp. 242–352, 2021. [Online]. Available: <https://opg.optica.org/aop/abstract.cfm?uri=aop-13-2-242>
- [6] A. J. Mercante, S. Shi, P. Yao, L. Xie, R. M. Weikle, and D. W. Prather, "Thin film lithium niobate electro-optic modulator with terahertz operating bandwidth," *Opt. Exp.*, vol. 26, no. 11, p. 14810, May 2018. [Online]. Available: <https://opg.optica.org/oe/abstract.cfm?uri=oe-26-11-14810>
- [7] G. Chen et al., "Compact slow-light waveguide and modulator on thin-film lithium niobate platform," *Nanophotonics*, vol. 12, no. 18, pp. 3603–3611, Sep. 2023, doi: [10.1515/nanoph-2023-0306](https://doi.org/10.1515/nanoph-2023-0306).
- [8] C. Haffner et al., "Low-loss plasmon-assisted electro-optic modulator," *Nature*, vol. 556, no. 7702, pp. 483–486, Apr. 2018. [Online]. Available: <https://www.nature.com/articles/s41586-018-0031-4>
- [9] X. Zhu et al., "Ultra wideband dual-output thin film lithium niobate intensity modulator," *IEEE J. Select. Topics Quantum Electron.*, vol. 30, no. 4, pp. 1–13, Aug. 2024. [Online]. Available: <https://ieeexplore.ieee.org/abstract/document/10496962>
- [10] Y. Qi et al., "Electro-optic frequency comb-enabled precise distance measurement with megahertz acquisition rate," 2023, *arXiv:2312.15743*.
- [11] S. Shi et al., "Ultrawideband modular RF frontend development for photonically enabled imaging receiver," *IEEE Microw. Wireless Technol. Lett.*, vol. 34, no. 6, pp. 805–808, Jun. 2024. [Online]. Available: <https://ieeexplore.ieee.org/abstract/document/10521887>
- [12] S. Nelan et al., "Compact thin film lithium niobate folded intensity modulator using a waveguide crossing," *Opt. Exp.*, vol. 30, no. 6, p. 9193, Mar. 2022. [Online]. Available: <https://opg.optica.org/oe/abstract.cfm?uri=oe-30-6-9193>
- [13] S. Sun et al., "Folded heterogeneous silicon and lithium niobate Mach-Zehnder modulators with low drive voltage," *Micromachines*, vol. 12, no. 7, p. 823, Jul. 2021. [Online]. Available: <https://www.mdpi.com/2072-666X/12/7/823>
- [14] G. Chen et al., "Compact 100GBaud driverless thin-film lithium niobate modulator on a silicon substrate," *Opt. Exp.*, vol. 30, no. 14, pp. 25308–25317, Jul. 2022. [Online]. Available: <https://opg.optica.org/oe/abstract.cfm?uri=oe-30-14-25308>
- [15] J. Hu et al., "Folded thin-film lithium niobate modulator based on a poled Mach-Zehnder interferometer structure," *Opt. Lett.*, vol. 46, no. 12, pp. 2940–2943, 2021. [Online]. Available: <https://opg.optica.org/ol/abstract.cfm?uri=ol-46-12-2940>
- [16] X. Liu et al., "Broadband meandered thin-film lithium niobate modulator with ultra-low half-wave voltage," *IEEE Photon. Technol. Lett.*, vol. 34, no. 8, pp. 424–427, Apr. 4, 2022. [Online]. Available: <https://ieeexplore.ieee.org/abstract/document/9749091>
- [17] X. Zhu et al., "Phase modulation using a titanium dioxide strip on lithium niobate," *Opt. Mater. Exp.*, vol. 12, no. 8, pp. 3296–3302, Aug. 2022. [Online]. Available: <https://opg.optica.org/ome/abstract.cfm?uri=ome-12-8-3296>
- [18] L. He, M. Zhang, A. Shams-Ansari, R. Zhu, C. Wang, and L. Marko, "Low-loss fiber-to-chip interface for lithium niobate photonic integrated circuits," *Opt. Lett.*, vol. 44, no. 9, p. 2314, May 2019. [Online]. Available: <https://opg.optica.org/ol/abstract.cfm?uri=ol-44-9-2314>
- [19] L.-W. Luo, G. S. Wiederhecker, J. Cardenas, C. Poitras, and M. Lipson, "High quality factor etchless silicon photonic ring resonators," *Opt. Exp.*, vol. 19, no. 7, pp. 6284–6289, Mar. 2011. [Online]. Available: <https://opg.optica.org/oe/abstract.cfm?uri=oe-19-7-6284>
- [20] Y. Zhang et al., "Systematic investigation of millimeter-wave optical modulation performance in thin-film lithium niobate," *Photon. Res.*, vol. 10, no. 10, p. 2380, Oct. 2022. [Online]. Available: <https://opg.optica.org/prj/abstract.cfm?uri=prj-10-10-2380>